Supporting Information

High Porosity in Nanostructured *n*-Type Bi_2Te_3 Obtaining Ultralow Lattice Thermal Conductivity

Yuan Wang,[1] Wei-Di Liu,[2] Han Gao,[2] Li-Jun Wang,[2] Meng Li,[2] Xiao-Lei Shi,[2] Min Hong,[1] Hao Wang,[1] Jin Zou,[2,3] and Zhi-Gang Chen[*,1,2]*

[1]Centre for Future Materials, University of Southern Queensland, Springfield central, Queensland 4300, Australia.

[2]Materials Engineering, The University of Queensland, Brisbane, Queensland 4072, Australia.

[3]Centre for Microscopy and Microanalysis, The University of Queensland, Brisbane, Queensland 4072, Australia

Corresponding author: [1] zhigang.chen@usq.edu.au, [2] zhigang.chen@uq.edu.au

1. Magnified XRD results of as-synthesized Bi_2Te_3 powder and as-sintered Bi_2Te_3 pellet

Te vacancy can be manifested from the peak shift in our magnified XRD results in the **Fig. S1**. Specifically, Te vacancy can lead lattice shrinkage in Bi_2Te_3 due to the absence of Te atoms. According to Bragg's Law, this will accordingly induce higher θ of the XRD peaks, which is reflected from the shifted (0 0 15) peaks of both powder and pellet samples towards higher degree.

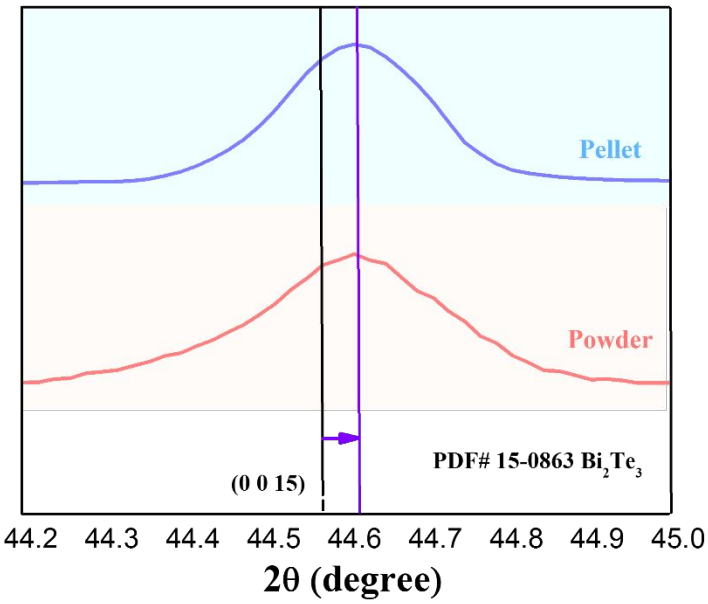

Fig. S1. Magnified XRD results of as-synthesized Bi_2Te_3 powder and as-sintered Bi_2Te_3 pellet, where peak shift towards higher degree is observed.

2. XPS spectra of as-synthesized Bi_2Te_3 powder and as-sintered Bi_2Te_3 pellet

Full X-ray spectroscopy (XPS) spectra of as-synthesized Bi_2Te_3 nano-powder and as-sintered porous nanostructured Bi_2Te_3 pellet are shown in **Fig. S2a** and **Fig. S2b**, respectively. The presences of Bi 4f and Te 3d energy states were exclusively determined, without any energy states detected for other elements, except C 1s and O 1s. Corresponding high-resolution XPS scans of Bi in the as-synthesized Bi_2Te_3 nano-powder and as-sintered porous nanostructured Bi_2Te_3 pellet are shown in **Fig. S2c** and **Fig. S2d**, respectively. No obvious difference was found after the sintering. The existence of single valence state Bi^{3+} in both Bi_2Te_3 nano-powder and porous nanostructured Bi_2Te_3 pellet was verified, where peaks of Bi $4f_{5/2}$ and Bi $4f_{7/2}$ were detected at 162.5 eV and 157.2 eV, respectively.[1]

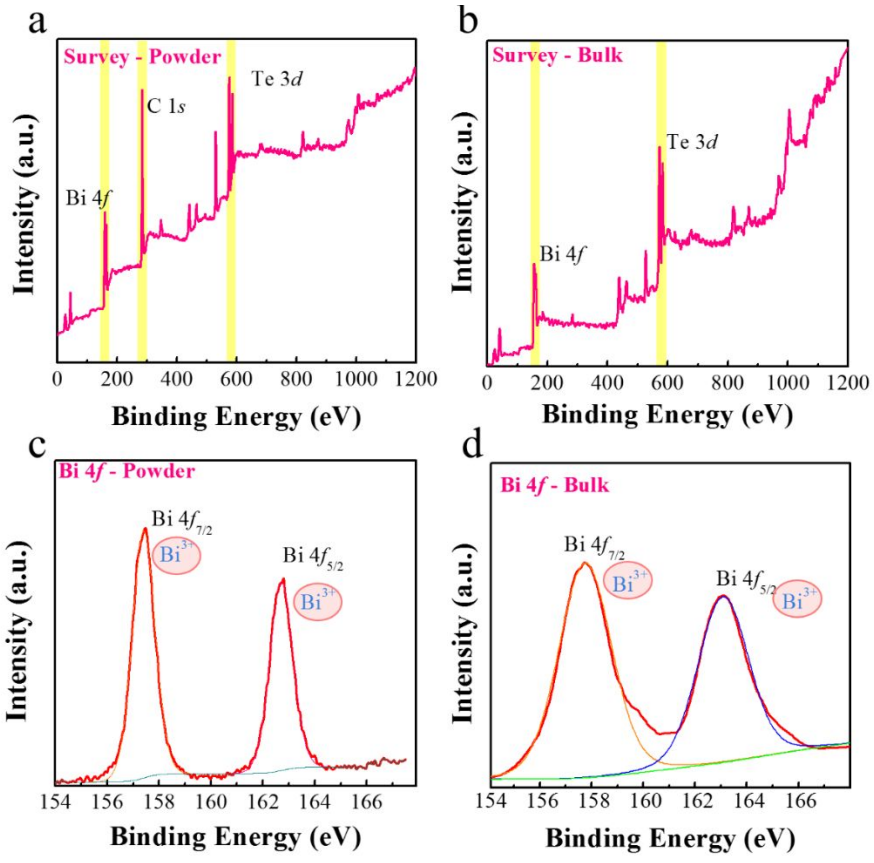

Fig. S2. Full XPS spectra of (a) as-synthesized Bi_2Te_3 nano-powder and (b) as-sintered porous nanostructured Bi_2Te_3 pellet. High-resolution XPS scans of Bi in the (c) as-synthesized Bi_2Te_3 nano-powder and (d) as-sintered porous nanostructured Bi_2Te_3 pellet.

3. Lorenz factor and measured thermal properties

Fig. S3a shows the SPB-calculated Lorenz factor (L) of as-sintered porous nanostructured Bi_2Te_3 pellet. L was found to be around 1.8×10^{-8} v^2 K^{-2}, with no obvious change within the temperature between 300 K and 550 K. **Fig. S3b** shows calculated electrical thermal conductivity (κ_e) of as-sintered porous nanostructured Bi_2Te_3 pellet. Similar values were found compared with dense nanostructured Bi_2Te_3 pellet.[2] **Fig. S3c** shows measured thermal diffusivity (D) of as-sintered porous nanostructured Bi_2Te_3 pellet. **Fig. S3d** shows measured heat capacity (C_p) of as-sintered porous nanostructured Bi_2Te_3 pellet, which is well consistent with dense nanostructured Bi_2Te_3 pellet.[2]

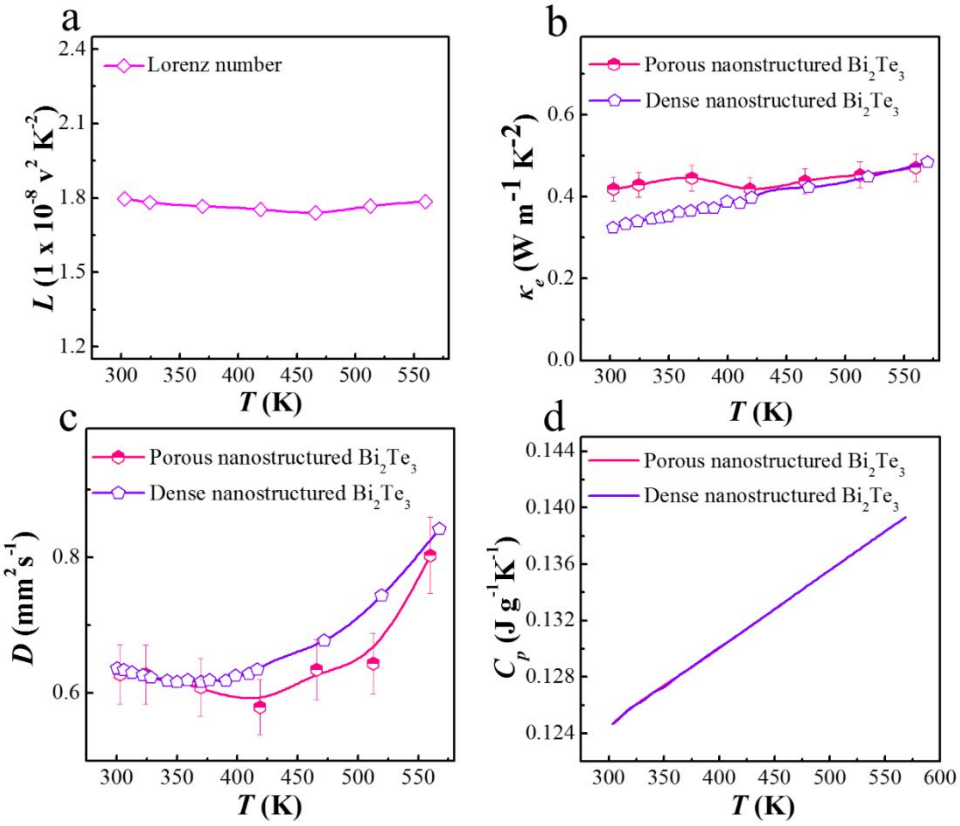

Fig. S3. (a) Calculated Lorenz factor with SPB model. T-dependent (b) κ_e; (c) D and (d) C_p of as-sintered porous nanostructured Bi_2Te_3 pellet and dense nanostructured Bi_2Te_3 pellet.[2]

4. EPMA results

Table S1 shows detailed atomic composition of as-sintered porous nanostructured Bi_2Te_3 pellet characterized by electron probe micro-analyzer (EPMA). Ten sites were randomly selected to ensure the reliability and accuracy of the pellet composition.

Table S1. EPMA measured atomic composition of as-sintered porous nanostructured Bi_2Te_3 pellet.

Point	Bi (at. %)	Te (at. %)	Total (at. %)	Bi/Te
1	35.2934	49.3951	100	0.714512
2	33.1585	46.3125	100	0.715973
3	33.2491	47.0595	100	0.706533
4	37.0272	50.6173	100	0.731513
5	36.3166	48.8793	100	0.742985
6	38.8218	55.1961	100	0.703343
7	39.0351	55.3944	100	0.704676
8	39.134	55.0341	100	0.711086
9	38.4345	54.9078	100	0.699983
10	38.5582	53.2736	100	0.723777
Average	36.90284	51.60697	100	0.715438

5. SPB model calculation details

We used a single parabolic band (SPB) model[3, 4] to calculate the enhancement of *n*-dependent *zT* with reduced lattice thermal conductivity (κ_l). For calculation details, the carrier transport property analysis was employed as:

$$S(\eta) = \frac{k_B}{e} \cdot \left[\frac{\left(r + \frac{5}{2}\right) \cdot F_{r+\frac{3}{2}}(\eta)}{\left(r + \frac{3}{2}\right) \cdot F_{r+\frac{1}{2}}(\eta)} - \eta \right] \tag{S4-1}$$

$$n = \frac{1}{e \cdot R_H} = \frac{(2m^* \cdot k_B T)^{\frac{3}{2}}}{3\pi^2 \hbar^3} \cdot \frac{\left(r + \frac{3}{2}\right)^2 \cdot F^2_{r+\frac{1}{2}}(\eta)}{\left(2r + \frac{3}{2}\right) \cdot F_{2r+\frac{1}{2}}(\eta)} \tag{S4-2}$$

$$\mu = \left[\frac{4\pi\hbar^4 C_l}{\sqrt{2}(k_B T)^{\frac{3}{2}} E^2_{Def} (m^*)^{\frac{5}{2}}} \right] \frac{\left(2r + \frac{3}{2}\right) \cdot F_{2r+\frac{1}{2}}(\eta)}{\left(r + \frac{3}{2}\right)^2 \cdot F_{r+\frac{1}{2}}(\eta)} \tag{S4-3}$$

$$L = \left(\frac{k_B}{e}\right)^2 \cdot \left\{ \frac{\left(r + \frac{7}{2}\right) \cdot F_{r+\frac{5}{2}}(\eta)}{\left(r + \frac{3}{2}\right) \cdot F_{r+\frac{1}{2}}(\eta)} - \left[\frac{\left(r + \frac{5}{2}\right) \cdot F_{r+\frac{3}{2}}(\eta)}{\left(r + \frac{3}{2}\right) \cdot F_{r+\frac{1}{2}}(\eta)} \right]^2 \right\} \tag{S4-4}$$

where η, k_B, e, r, R_H, $\hbar$, C_l, E_{def}, and L are the reduced Fermi level, the Boltzmann constant, the electron charge, the carrier scattering factor (r = -1/2 for acoustic phonon scattering), the Hall coefficient, the reduced plank constant, the elastic constant for longitudinal vibrations, the deformation potential coefficient, and the Lorenz number, respectively. Here:

$$C_l = v_l^2 \cdot \rho \tag{S4-5}$$

where v_l is the longitudinal sound velocity and taken as 2884 m s^{-1} in this study.[5] $F_i(\eta)$ is the Fermi integral expressed as:

$$F_i(\eta) = \int_0^\infty \frac{x^i}{1 + e^{(x-\eta)}} dx \tag{S4-6}$$

To predict the *zT* enhancement with reduced κ_l by inducing porous structure, we assume that the pores are uniformly distributed in the Bi_2Te_3 matrix. In this situation, κ_{lp} can be defined as

the κ_l of porous Bi_2Te_3. Here, experimentally measured κ_l was utilized. Phonon mean free path Λ_b was calculated as:[6]

$$\Lambda_b = \frac{3 \cdot \kappa_{lb}}{C_v v_\alpha} \tag{S4-7}$$

where C_v is the volume heat capacity. v_α is the average sound velocity taken as 2147 m s^{-1}.[5]

6. A comprehensive comparison of *zT* with other state-of-art binary *n*-type Bi_2Te_3 works

A comprehensive comparison with other state-of-art binary *n*-type Bi_2Te_3 works can be found from **Fig. S4**, where the achieved *zT* of 0.97 in our work is listed as one of the highest values reported for binary *n*-type Bi_2Te_3.

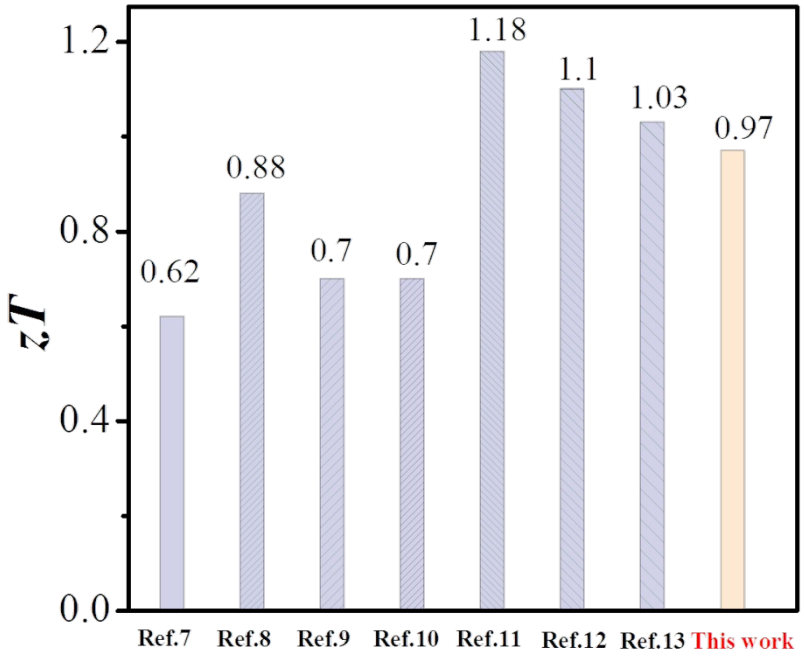

Fig. S4. A comprehensive comparison of *zT* with other state-of-art binary *n*-type Bi_2Te_3 works.[7-13]

Reference

1 J. Fu, S. Song, X. Zhang, F. Cao, L. Zhou, X. Li and H. Zhang, *CrystEngComm*, 2012, **14**, 2159-2165.

2 L. Yang, Z. G. Chen, M. Hong, G. Han and J. Zou, *ACS Appl. Mater. Interfaces*, 2015, **7**, 23694-23699.

3 Y. Xu, W. Li, C. Wang, J. Li, Z. Chen, S. Lin, Y. Chen and Y. Pei, *J. Mater. Chem. A*, 2017, **5**, 19143-19150.

4 X. She, X. Su, H. Du, T. Liang, G. Zheng, Y. Yan, R. Akram, C. Uher and X. Tang, *J. Mater. Chem. C*, 2015, **3**, 12116-12122.

5 M. Hong, T. C. Chasapis, Z. G. Chen, L. Yang, M. G. Kanatzidis, G. J. Snyder and J. Zou, *ACS Nano*, 2016, **10**, 4719-4727.

6 K. Zhao, H. Duan, N. Raghavendra, P. Qiu, Y. Zeng, W. Zhang, J. Yang, X. Shi and L. Chen, *Adv. Mater.*, 2017, **29**, 1701148.

7 Yang, L.; Chen, Z. G.; Hong, M.; Han, G.; Zou, J. Enhanced Thermoelectric Performance of Nanostructured Bi_2Te_3 through Significant Phonon Scattering. *ACS Appl. Mater. Interfaces* **2015,** *7*, 23694-23699.

8 Zhang, Y.; Day, T.; Snedaker, M. L.; Wang, H.; Kramer, S.; Birkel, C. S.; Ji, X.; Liu, D.; Snyder, G. J.; Stucky, G. D. A mesoporous anisotropic *n*-type Bi_2Te_3 monolith with low thermal conductivity as an efficient thermoelectric material. *Adv. Mater.* **2012,** *24*, 5065-5070.

9 Fu, J.; Song, S.; Zhang, X.; Cao, F.; Zhou, L.; Li, X.; Zhang, H. Bi_2Te_3 Nanoplates and Nanoflowers: Synthesized by Hydrothermal Process and their Enhanced Thermoelectric Properties. *CrystEngComm* **2012,** *14*, 2159-2165.

10 Yu, F.; Xu, B.; Zhang, J.; Yu, D.; He, J.; Liu, Z.; Tian, Y. Structural and thermoelectric characterizations of high pressure sintered nanocrystalline Bi2Te3 bulks. *Mater. Res. Bull* **2012,** *47*, 1432-1437.

11 Son, J. S.; Choi, M. K.; Han, M. K.; Park, K.; Kim, J. Y.; Lim, S. J.; Oh, M.; Kuk, Y.; Park, C.; Kim, S. J.; Hyeon, T. *n*-Type Nanostructured Thermoelectric Materials Prepared from Chemically Synthesized Ultrathin Bi_2Te_3 Nanoplates. *Nano Lett.* **2012,** *12*, 640-647.

12 Mehta, R. J.; Zhang, Y.; Karthik, C.; Singh, B.; Siegel, R. W.; Borca-Tasciuc, T.; Ramanath, G. A new class of doped nanobulk high-figure-of-merit thermoelectrics by scalable bottom-up assembly. *Nat. Mater.* **2012,** *11*, 233-240.

13 Zhao, L. D.; Zhang, B. P.; Li, J. F.; Zhang, H. L.; Liu, W. S. Enhanced thermoelectric and mechanical properties in textured *n*-type Bi_2Te_3 prepared by spark plasma sintering. *Solid State Sci.* **2008,** *10*, 651-658.